ELSEVIER

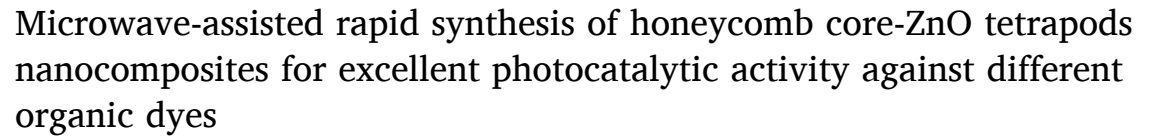
Contents lists available at ScienceDirect

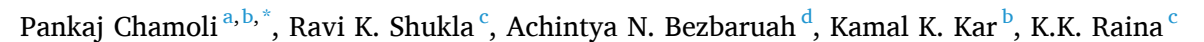
Applied Surface Science

journal homepage: www.elsevier.com/locate/apsusc



Full Length Article





- a School of Basic & Applied Sciences, Department of Physics, Shri Guru Ram Rai University, Dehradun 248001, Uttarakhand, India
- b Advanced Nanoengineering Materials Laboratory, Materials Science Programme, Indian Institute of Technology Kanpur, Kanpur 208016, India
- ^c Advanced Functional Smart Materials Laboratory, School of Physical Sciences, Department of Physics, DIT University, Debradum 248009, Uttarakhand, India
- d Nanoenvirology Research Group, Civil and Environmental Engineering, North Dakota State University, Fargo, ND 58105, United States

ARTICLE INFO

Keywords: Microwave irradiation Exfoliated graphite Graphene nanocomposites ZnO tetrapods Photocatalytic activity

ABSTRACT

Microwave-assisted rapid approach (300 W, 180 s) has been demonstrated for the synthesis of graphene nanosheets (GNs)-zinc oxide (ZnO) nanocomposites. It is noted that the microwave process not only fastens the nucleation and growth but also gives better control to engineer anisotropic nanostructure over a carbon core. In the studied system, surface morphological analysis reveals the well-defined growth of a ZnO tetrapods (TPs) nanostructure over the carbon core (graphene). Raman signature confirms the formation of GNs-ZnO tetrapods (GZnTPs) nanocomposites with a tri-layered GNs system. GZnTPs exhibits a lower bandgap (3.09 eV) than that of pure EG and ZNTPs. Best photocatalytic activities are noticed for the GZnTPs owing to the recombination of photogenerated electrons. GZnTPs are tested for their ability to photodegrade Rhodamine B (RhB), Methyl orange (MO), and Methylene blue (MB) dyes under UV and visible (both 125 W) light irradiation. GZnTPs act as excellent photocatalysts for RhB with a maximum degradation efficiency of 91.6% under UV light irradiation and stable for three cycles.

1. Introduction

Technological development not only improving the living standard of humankind but also destroying the ecological system. Waste products from the industries (i.e. textile, paper, plastic, packaging, etc.) containing hazardous pollutants (i.e. organic dyes, heavy metal ions, etc.) are being dumped in our aquatic system and severely affecting it [1-2]. The remediation of these organic pollutants/dves is being carried out through photo-decomposition using different photocatalyst (e.g. metal oxides, carbon material, etc.) [3-6]. Since the discovery, graphene: single-atom-thick carbon sheets arranged in a two-dimensional honeycomb lattice has been grabbed wide attention due to its exceptional properties such as excellent room temperature carrier mobility \sim 200,000 cm² V⁻¹ s⁻¹, high optical transmittance \sim 97.7%, large surface area \sim 2630 m²/g, fracture strength \sim 130 GPa, high flexibility, and excellent thermal conductivity $\sim 5000 \text{ W m}^{-1} \text{ K}^{-1}$ [7,8]. Therefore, graphene has shown potential applications in the field of photochemistry, nanoscience, and engineering [9-11]. Various methods have been

reported for the synthesis of graphene nanosheets (GNs) which include chemical vapor deposition (CVD) [12], arch discharge [13], and wet chemistry routes [14]. Among these methods, wet chemistry GNs synthesis routes are widely used due to their simplicity, cost-effectiveness, and high yield [15,16]. In recent years, different nanoparticles (ZnO, CdS, TiO₂, and SnO₂) have been decorated over the graphene (carbon core) for various applications [17–20]. In particular, Zinc oxide (ZnO, wide bandgap \sim 3.37 eV) is used widely due to its ease of production, and low toxicity; and investigated wieldy for various other applications such as ultraviolet (UV) lasers, sensors, solar cells, and as a photocatalyst [21–23]. Despite having a wide bandgap, the photocatalytic efficiency of ZnO is found low which may be due to the recombination of the photo-induced electron-hole pairs [24], However, its combination with GNs not only improves the photocatalytic performance but also prevents the recombination of photo-generated electron-hole pairs [25]. Therefore, carbon-metal nanocomposites (NCs) have been promoted by researchers for their potential for photocatalytic activities. Specifically, a number of studies have reported the use of ZnO decorated over carbon

^{*} Corresponding author at: School of Basic & Applied Sciences, Department of Physics, Shri Guru Ram Rai University, Dehradun 248001, Uttarakhand, India. E-mail address: pchamoli83@gmail.com (P. Chamoli).

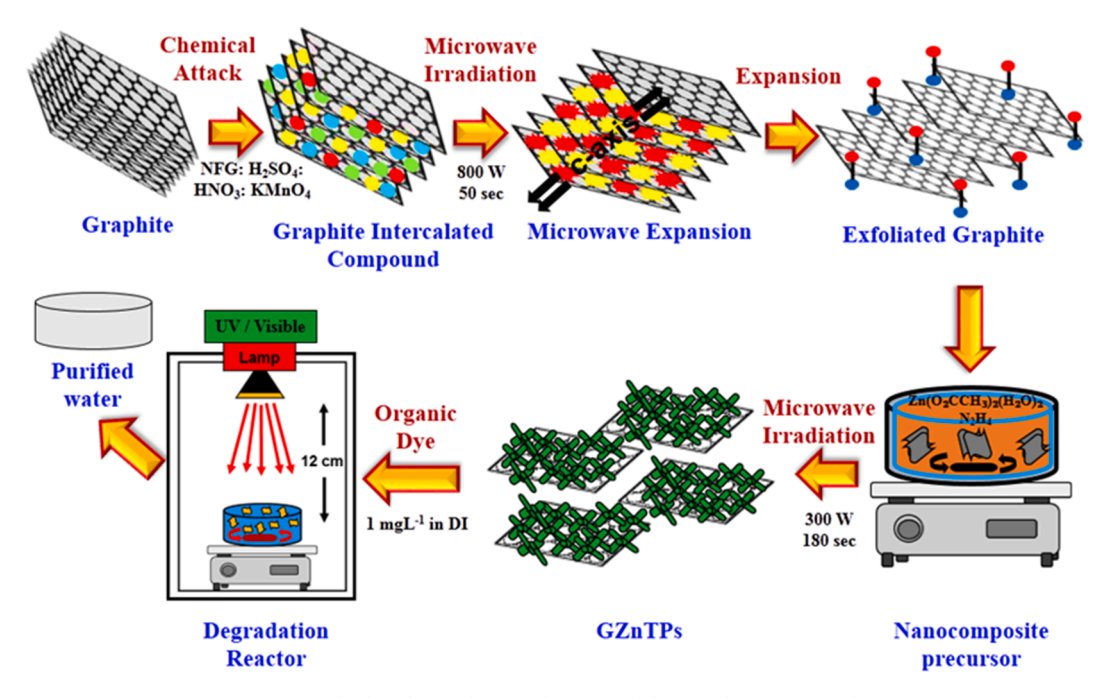


Fig. 1. Steps involved in the synthesis and testing of photocatalytic activity of GZnTPs.

core as a photocatalyst to degrade pollutants from textile industries. For example, zinc oxide-reduced graphene oxide (ZnO/rGO) NCs have been synthesized by Fan et al. using the hydrothermal method, and tested for photocatalytic degradation of methylene blue (MB), methylene orange (MO), and Rhodamine (RhB) under ultraviolet (UV) light irradiation (150 W). The results show that degradation efficiency (DE) of \sim 99% is achieved in 30 min [25]. Ravi et al. also prepared ZnO/rGO NCs using the hydrothermal method, and tested their photocatalytic activity under UV with Congo red (CR) and Eosin yellow (EY) as the target contaminants. They achieved up to 98% removal of the dyes in 90 min [26]. Similarly, Jabeen et al. have achieved 68% removal of MB in 120 min under UV light (500 W) using ZnO/rGO NCs [27]. Moreover, a ternary ZnO/CuO/rGO NCs have also been synthesized via the solid-state method and studied for the removal of RhB, and 99% DE is achieved in 20 min under visible light (150 W) [28]. These NCs worked effectively as photocatalysts; however, their preparation methods are tedious and energy-intensive [29]. Microwave synthesis is reported to be effective for rapid and controlled nucleation and growth of nanomaterials, and it is less energy-intensive than other methods [30]. However, microwaveassisted synthesis methods have not been explored extensively for NCs preparation.

The present work was an attempt to rapidly grow ZnO anisotropic tetrapods (TPs) over graphene to prepare graphene-zinc oxide tetrapod NCs (GZnTPs). We hypothesized that the multifaceted anisotropic structure would have enhanced photocatalytic activities owing to their direction-oriented properties and functionalities. The GZnTPs were further evaluated for photocatalytic properties via degradation of three organic dyes [methylene blue (MB), methylene orange (MO), and Rhodamine B (RhB)] under UV and visible light irradiations.

2. Experimental

2.1. Materials

Natural flakes graphite (NFG) (99.9% pure, Sigma Aldrich) was used for the synthesis of exfoliated graphite (EG). Zinc acetate dihydrate (Zn $(O_2CCH_3)_2(H_2O)_2$, 98%), potassium permanganate (KMnO₄, 99%), hydrazine hydrate (N₂H₄, 99%), nitric acid (HNO₃, 63%), and sulphuric acid (H₂SO₄, 98%) were procured from Qualigens Fine Chemicals Ltd.

(India). Rhodamine B (RhB), Methyl orange (MO), and Methylene blue (MB) dyes were procured from Loba Chemie Pvt. Ltd. (India). All materials were used received unless otherwise specified.

2.2. Preparation of EG

The exfoliation of NFG was carried out using a dry process as per Chamoli $\it et al.$ [31]. Briefly, the graphite intercalation compound (GIC, a mixture of various strong acids and oxidizing agents) was used as the precursor material for the synthesis of EG. In this exfoliation process, NFG was mixed with sulphuric acid (H $_2SO_4$), nitric acid (HNO $_3$), and potassium permanganate (KMnO $_4$) in a porcelain dish for 10 s using a glass rod in the weight ratio 1:1:1:1 (NFG: H $_2SO_4$: HNO $_3$: KMnO $_4$) at 25 $^\circ$ C to get GIC. The GIC was then transferred to a 250 mL glass beaker and placed in a commercially available domestic microwave oven (Samsung, 2448 MHz, variable up to 800 W). The precursor was then cooked (treated) with microwave irradiation at 800 W for 50 s to exfoliate the NFG to form EG.

2.3. Preparation of GZnTPs

First, ZnO tetrapods (ZnTPs) were synthesized by microwaving (300 W, 180 s) a mixture of Zn $(O_2CCH_3)_2(H_2O)_2$ and N_2H_4 (1:4 M ratio) [32]. Once the formation of ZnTPs was confirmed by electron microscopic (FESEM) analysis (Fig. S1), the GZnTPs were synthesized as follows. EG (0.2 mg/mL) was mixed in 100 mL deionized (DI) water and sonicated for 3 h to achieve homogenous dispersion. Thereafter, Zn (O₂CCH₃)₂(H₂O)₂ and N₂H₄ were mixed (1:4 M ratio) in the EG solution under continuous stirring. N₂H₄ instantly reacted with Zn (O₂CCH₃)₂(H₂O)₂ to form a slurry-like precipitate. The mixture was stirred for 0.5 h to ensure that the reaction was complete. Then the resultant mixture was transferred to the microwave oven (300 W, 180 s) for further reaction. The slurry became clear with a greyish precipitate settled to the bottom. The greyish precipitate was filtered using a $0.2\,\mu m$ membrane filter and washed several times with ethanol and a copious amount of DI water. The resultant filtrate was dried overnight in a vacuum oven at 80 °C to get GZnTPs. The synthesized NCs (GZnTPs) were characterized and tested for photocatalytic behavior (Fig. 1).

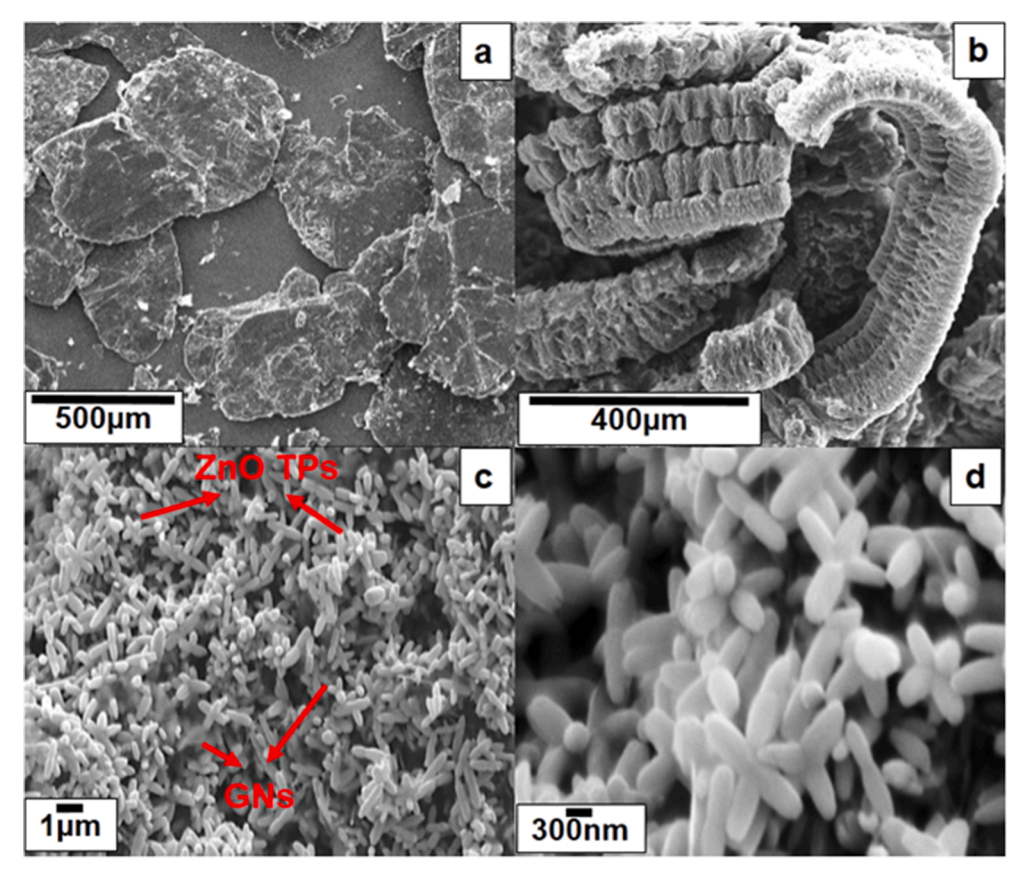


Fig. 2. FESEM micrograph of (a) NFG, (b) EG, and (c-d) GZnTPs.

2.4. Photocatalytic activity

Photocatalytic activities of the synthesized NCs (GZnTPs) were measured via separate photo-decomposition studies of three different organic dyes, namely RhB, MO, and MB (1 mg/L). For the photodecomposition experiment, GZnTPs (0.1 or 0.2 mg/L) was added to an aqueous solution of organic dyes (100 mL, 1 mg/L). The reactors were kept in a dark place with continuous stirring for 0.25 h to homogenize the mixture of the specific dye by the NCs. The reactors were then transferred to a custom-made UV/visible light irradiation chamber and were exposed to UV (wavelength ~365 nm, 125 W) or visible light (125 W) for a definite period. The working distance between the light source and the top of the reactor was kept as 12 cm based on preliminary optimization. Photocatalytic degradation behaviors of RhB, MB, and MO were monitored by measuring the dye concentration in the bulk solution over time (t). A UV-vis spectrophotometer (Perkin Elmer Lambda 365) was used to measure dye concentration (at $\lambda_{max} \sim 663$ nm) and calculated as $\frac{c_o-c_t}{c_o} \times 100\%$, where C_0 is the initial (t = 0) dye concentration and Ct is the concentration of the dyes at time t.

2.5. Characterization

The crystalline phase of NFG, EG, ZnTPs, and GZnTPs was recorded through X-ray diffraction (XRD) using X'Pert Powder PANalytical, Advanced X-Ray Diffractometer. Raman analysis of ZnTPs and GZnTPs was recorded by LabRam Micro-Raman spectrometer (Jobin-Yvon HR 800 UV) using a He-Ne (632.8 nm) laser excitation source. The morphology of the specific nanostructure was examined using a field emission scanning electron microscopy (FESEM, Zeiss EVO-50) and a transmission electron microscope (TEM, FEI Titan G2 60-300). The bond stretching in EG and GZnTPs in the range of 4000–400 cm⁻¹ were analyzed by Fourier transform infrared spectroscopy (Bruker-FTIR)

using a KBr pellet. The elemental analysis of EG and GZnTPs was carried out by X-ray photoelectron spectroscopy (XPS) with spectra acquired with a PHI500 (Versa ProbeII, FEI Inc.) with Al K α (1486.6 eV) X-ray source. Brunauer-Emmett–Teller (BET) method was used to find the specific surface area of ZnTPs and GZnTPs with an automatic instrument Quantachrome (ASiQwin).

3. Results and discussion

3.1. Morphological analysis

FESEM micrograph of NFG (Fig. 2a) shows a plate-like structure having a diameter of $\sim\!450\,\mu m$. A worm-shaped microstructure has been seen for EG (Fig. 2b) which is comprised of several oxygenated graphene layers (more detail about oxygenated layers is given in a subsequent section). The ZnO has formed unique tetrapods (TPs) structure having lengths of facets in the range of 200–500 nm (Fig. 2c–d). The shape of the present ZnO is unique compared to the others synthesized via microwave-assisted reaction [Supplementary Information (SI), Table S1].

The ZnO NCs consist of randomly crumpled thin sheets of GNs with ZnTPs. This confirms the formation of ZnTPs on the surfaces of GNs. The FESEM micrographs of GZnTPs reveal that the average diameter of ZnTPs is ~ 300 nm of prongs (Fig. 2d). The formation of nanostructure in microwave-assisted growth not only depends upon the microwave parameters (power, radiation energy, temperature, and reaction time) but also on the solvent and precursors properties such as polarity of the solvent, the concentration of the precursor, pH, nature of the reducing agent, and surface modifying agents [33–35]. Microwave radiation usually affects the chemical reactions and penetration of chemicals, and thus not only initiates the nucleation process but also enhances crystallite growth [35]. In the present study, N_2H_4 acted as a reducing agent and a complexing agent at the same time. $Zn(OH)_2$ is formed initially

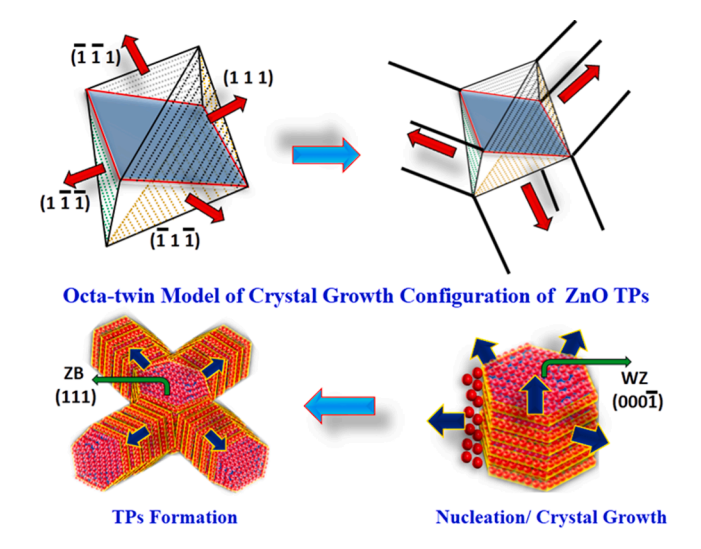


Fig. 3. Possible growth mechanism of ZnTPs under microwave irradiation (modified after Shiojiri $et\ al.\ [38]$.

(Eq. (1)) due to the addition of N_2H_4 to $Zn~(O_2CCH_3)_2(H_2O)_2$, and the produced $Zn(OH)_2$ is further dissociated to Zn^{2+} and OH^- ions (Eq. (2)) leading to the formation of ZnO~(Eq.~(3))~[34].

$$Zn(O_2CCH_3)_2.(H_2O)_2 + N_2H_4 + H_2O \rightarrow Zn(OH)_2 + CH_3COON$$
 (1)

$$Zn^{2+} + 2OH^{-} \xrightarrow{Microwave} Zn(OH)_2$$
 (2)

$$Zn^{2+} + 2OH^{-} \rightarrow 2ZnO + 2H^{+}$$
 (3)

Equation (3) represents the direct precipitation of the ZnO nuclei in the solution These nuclei are linked further to grow in the multiple lattices of a common connection. Each crystal grows along the c-axis which in turn leads to the formation of TPs with multi-faceted morphologies (Fig. 3). The growth of such TPs in the vicinity of EG in the microwaveassisted synthesis could be the result of the fusion of particles at the collision point and the growth of more primary complexes. The pH of the solution also plays an important role to control the morphology or in the growth of complex multi-facets tetrapod structures [36]. It is reported that pH > 11 is optimal for the growth of nanostructures with a higher aspect (length to diameter) ratio [37]. In our study, the overall pH of the microwaved solution was ~14. The N₂H₄ is a strong base with a pH of ~11, and the exfoliated graphite also contains hydroxyl groups at the surface to boost up the pH of the reaction mixture. The highly basic pH of the studied systems could also be a reason for the growth of multifaceted tetrapod structures.

Working with micromaterials, Shiojiri *et al.* [38] reported the formation of ZnTPs via rapid growth along with four $\langle 1\ 1\ \rangle$ directions perpendicular to the $\{1\ 1\ 1\}$ /Zn faces. They proposed a mechanism where wurtzite crystals are formed on their $\{1\ 1\ 1\}$ faces by introducing stacking faults, and they cultivate easily along their [0001] directions to produce ZnTPs and named the mechanism as an octa-twin model for crystal growth (Fig. 3) [38]. Nishio *et al.* [39] expanded the work by Fujii *et al.* [40] and indicated that multiple twins of nuclei are responsible for the growth ZnTPs. Our results vindicate that such simple microwave methodologies can also be utilized to engineer complex tetrapod-like multifaceted structures rather than using tedious

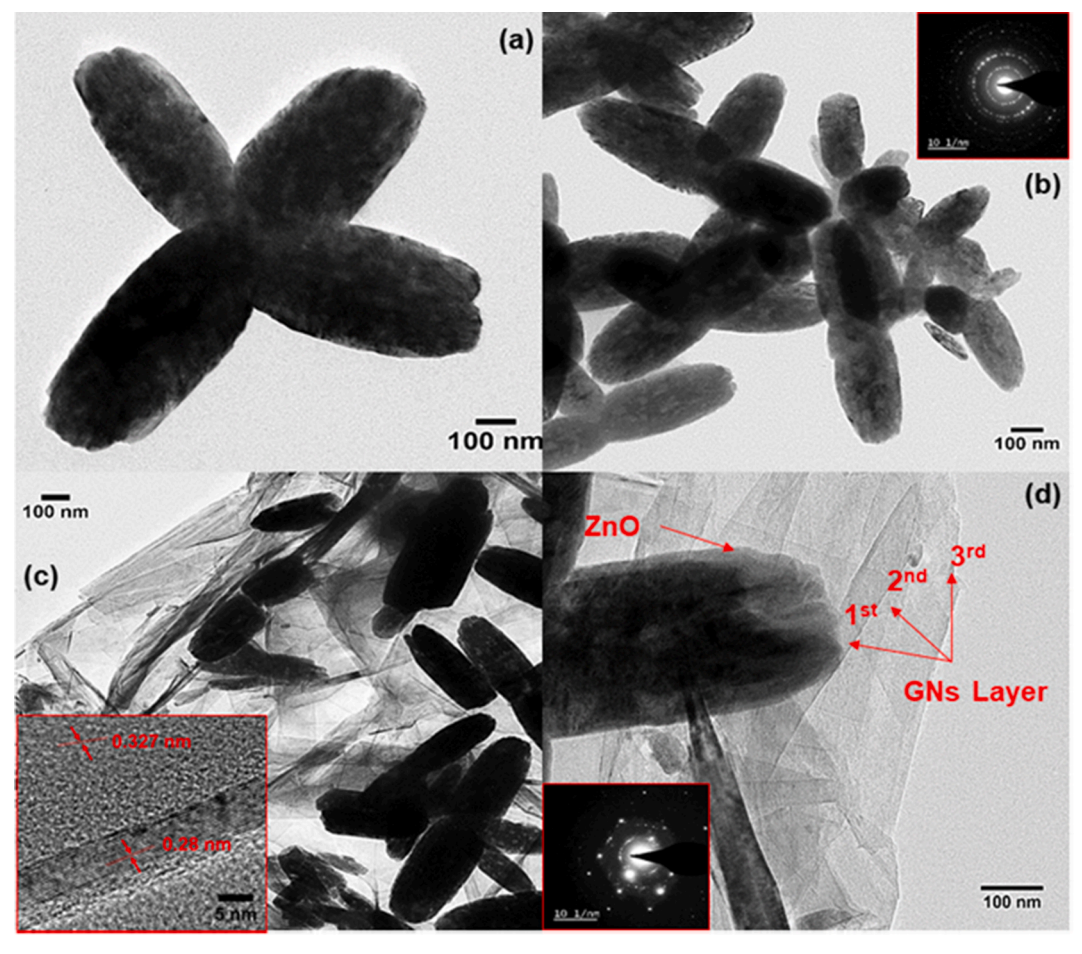


Fig. 4. TEM micrograph of (a, b) ZnTPs (Inset: SEAD pattern); (c) GZnTPs (Inset: high magnification); and (d) GZnTPs showing GNs layers (Inset: SEAD pattern).

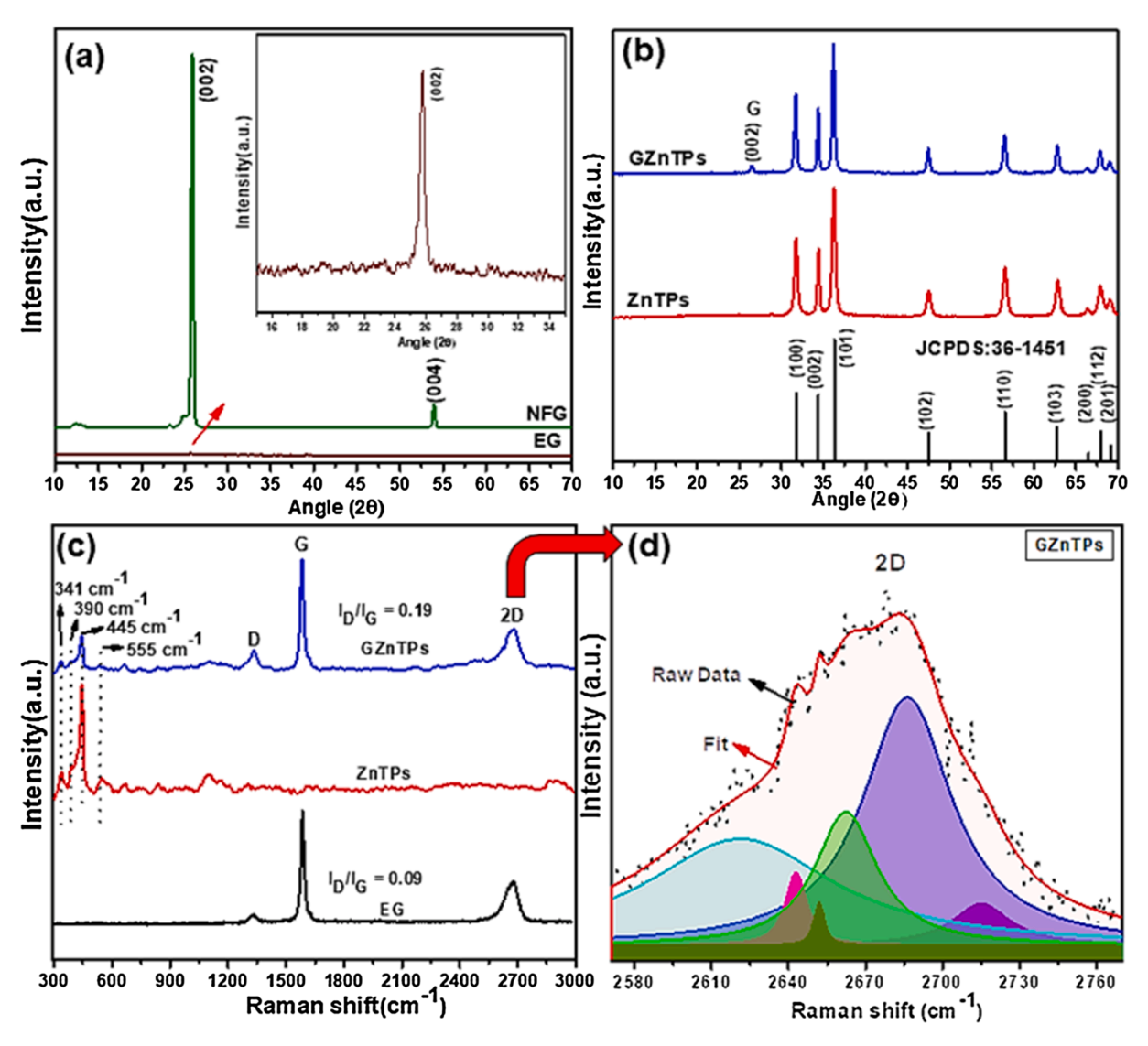


Fig. 5. (a) XRD patterns of NFG and EG, Inset: magnified EG peak; (b) XRD patterns of ZnTPs and GZnTPs; (c) Raman spectra of EG, ZnTPs, and GZnTPs; and (d) 2D peaks of GZnTPs well fitted with six Lorentz curves.

catalytic and surfactant mediated synthesis. Lower temperature, lower power, and shorter reaction time (180 s) in our approach might have been achieved because of the high polarity of the solvent.

Further, the TEM micrographs of ZnTPs and GZnTPs show stacking of GNs (Fig. 4). ZnTPs are uniform in size and shape having four awlshaped prongs arrangements. These prongs are gradually impending from a common core to the outside with an average angle of about 72° between the neighboring arms. The TP prongs are found to be 516–576 nm in length along the growth direction with an average diameter of 294 nm (Fig. 4ab). The diameters of prongs are gradually shrunk and that is very common for TPs with long prong lengths [41]. Well-faceted morphology has been observed at the junction indicating that no lattice mismatch occurred after the nucleation of ZnO in the central region. The growth mechanism has been already discussed (Fig. 3) and the TP growth happens due to the formation of wurtzite crystals on their {1 1 1} faces by introducing stacking faults and their easy cultivation along with their [0001] directions. The selected area electron diffraction pattern (SAED) confirms these plan formations (Fig. 4b: Inset). However, TEM micrographs of GZnTPs (Fig. 4cd) show that the acceptable quantity of ZnTPs have been grown over GNs. Awl-shaped prongs of ZnO have been found to be 289-414 nm in length. The average diameter of prongs is 174 nm and gradually shrunk in the growth direction from the core (Fig. 4cd). Additionally, the TEM image depicts that the GNs are having curled edges and several micrometers in size. The SAED shows a clear hexagonal electron diffraction pattern of graphene lattice (Fig. 4d: Inset). The number of layers is measured of the GNs, and a three-layered GNs system is found (Fig. 4d). The interlayer spacing of GNs is $\sim\!0.327$ nm which is in agreement with the d-spacing value reported in the literature for the few-layer GNs (Fig. 4c: Inset) [42]. Additionally, the specific surface area of ZnTPs and GZnTPs have been evaluated by the BET method using N2 adsorption/desorption isotherms at 77.35 K. Firstly, ZnTPs and GZnTPs have been degassed in N2 for 8 Hours at 200 °C under vacuum. The specific surface areas were calculated and found 11.25 m²/g for ZnTPs and 126.02 m²/g GZnTPs (SI, Fig.S2). These values are in agreement with reported values of the surface area of ZnO (multi-facet system, 0.90 m²/g) and ZnO/GNs based nanocomposites (115.70 m²/g) [43,44].

3.2. Structural analysis

The crystalline phases of NFG, EG, ZnTPs, and GZnTPs were recorded through X-ray diffraction (XRD) Fig. 5 (a, b). The XRD pattern of NFG shows a sharp intense peak at $2\theta=25.92^{\circ}$, denoting the crystalline structure [(0 0 2) plane] of hexagonal graphite (d=3.41 nm). The XRD pattern of EG shows an intense peak at $2\theta=25.76^{\circ}$ (d=3.43 nm) which is further matched with reported data by Sykam *et al.* [45]. The

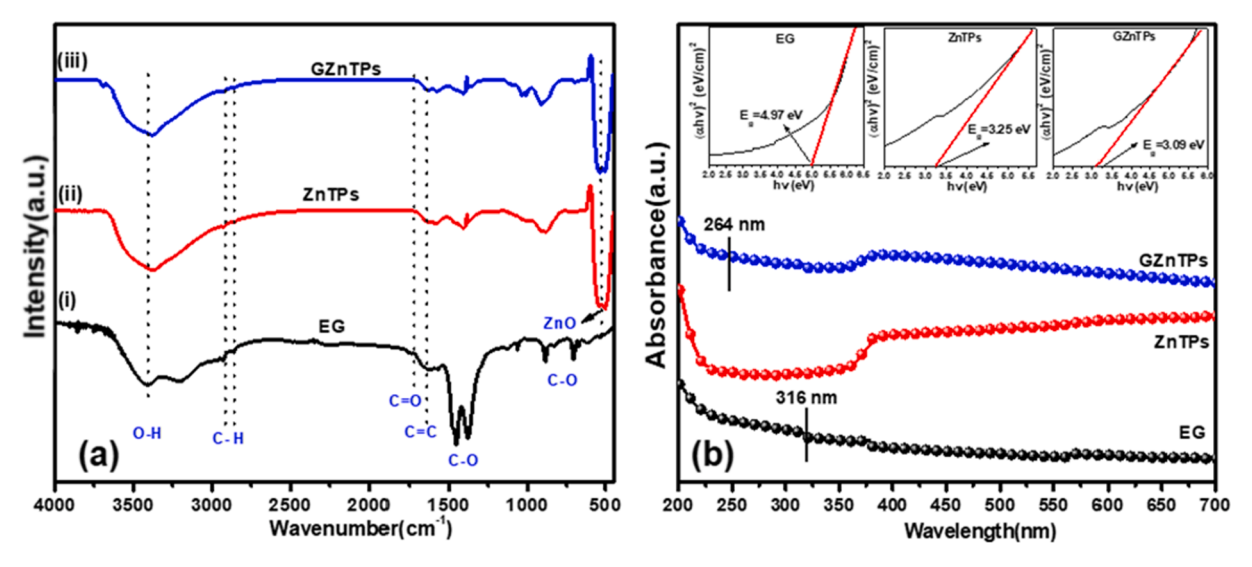


Fig. 6. (a) FTIR spectra of (i) EG, (ii) ZnTPs, and (iii) GZnTPs; (b) UV-vis spectra of EG, ZnTPs, and GZnTPs, Inset: Band gap calculation.

increased *d*-spacing indicates the exfoliation of graphite along the c-axis. In addition, XRD patterns of ZnTPs comprise nine peaks appearing at $2\theta = 31.75$, 34.43, 36.25, 47.46, 56.59, 62.92, 66.47, 67.92, and 69.01°, corresponding to the crystal planes (1 0 0), (0 0 2), (1 0 1), (1 0 2), (1 1

0), (1 0 3), (2 0 0), (1 1 2), and (2 0 1), respectively. These peaks are indexed with wurtzite-structured of ZnO (*JCPDS No. 36-1451*) [46]. The XRD pattern of GZnTPs composite exhibits all corresponding diffraction peaks of the wurtzite structure of ZnO and less intense graphene peak (0

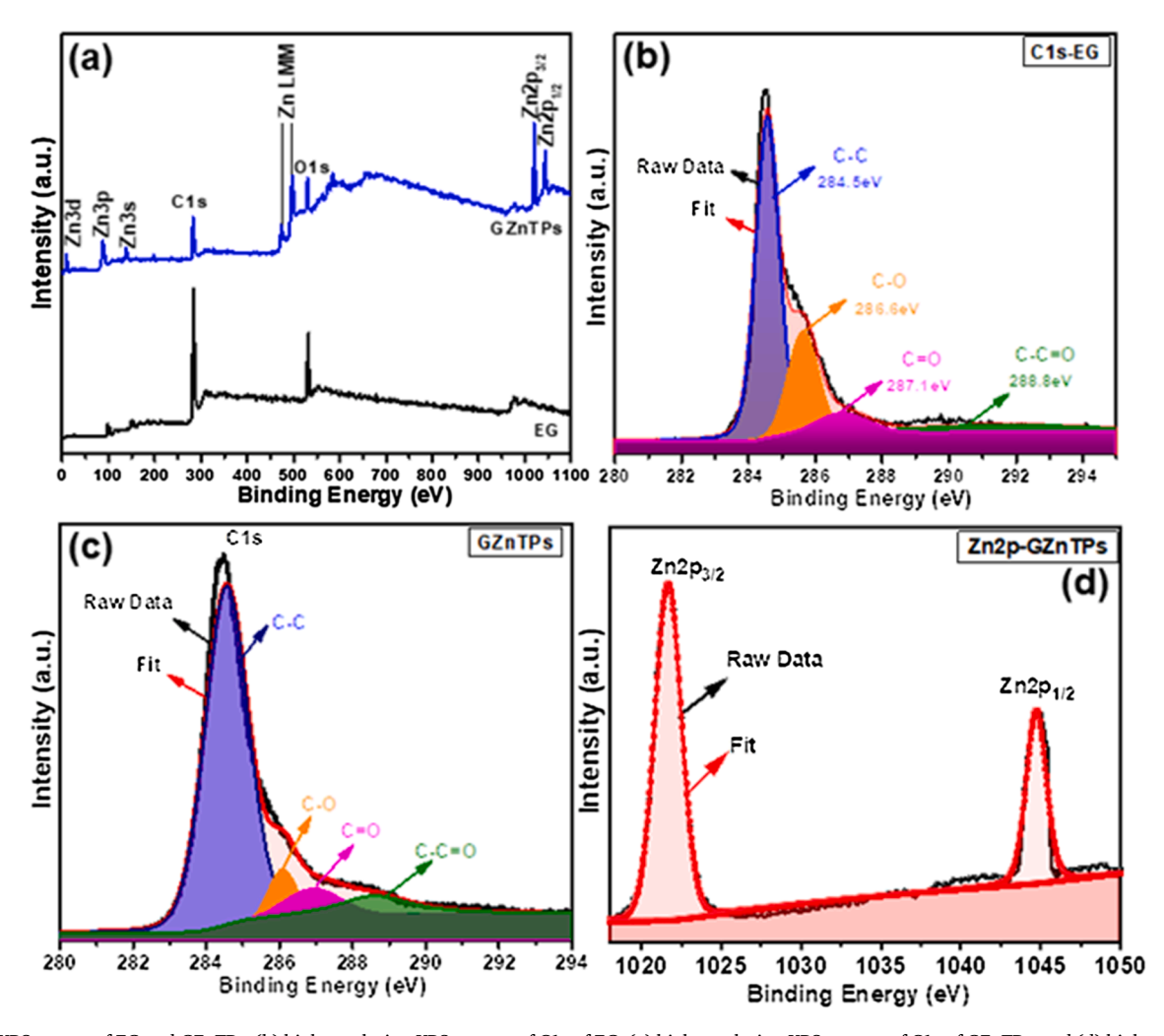


Fig. 7. (a) XPS survey of EG and GZnTPs; (b) high-resolution XPS spectra of C1s of EG; (c) high-resolution XPS spectra of C1s of GZnTPs; and (d) high-resolution XPS spectra of Zn2p of GZnTPs.

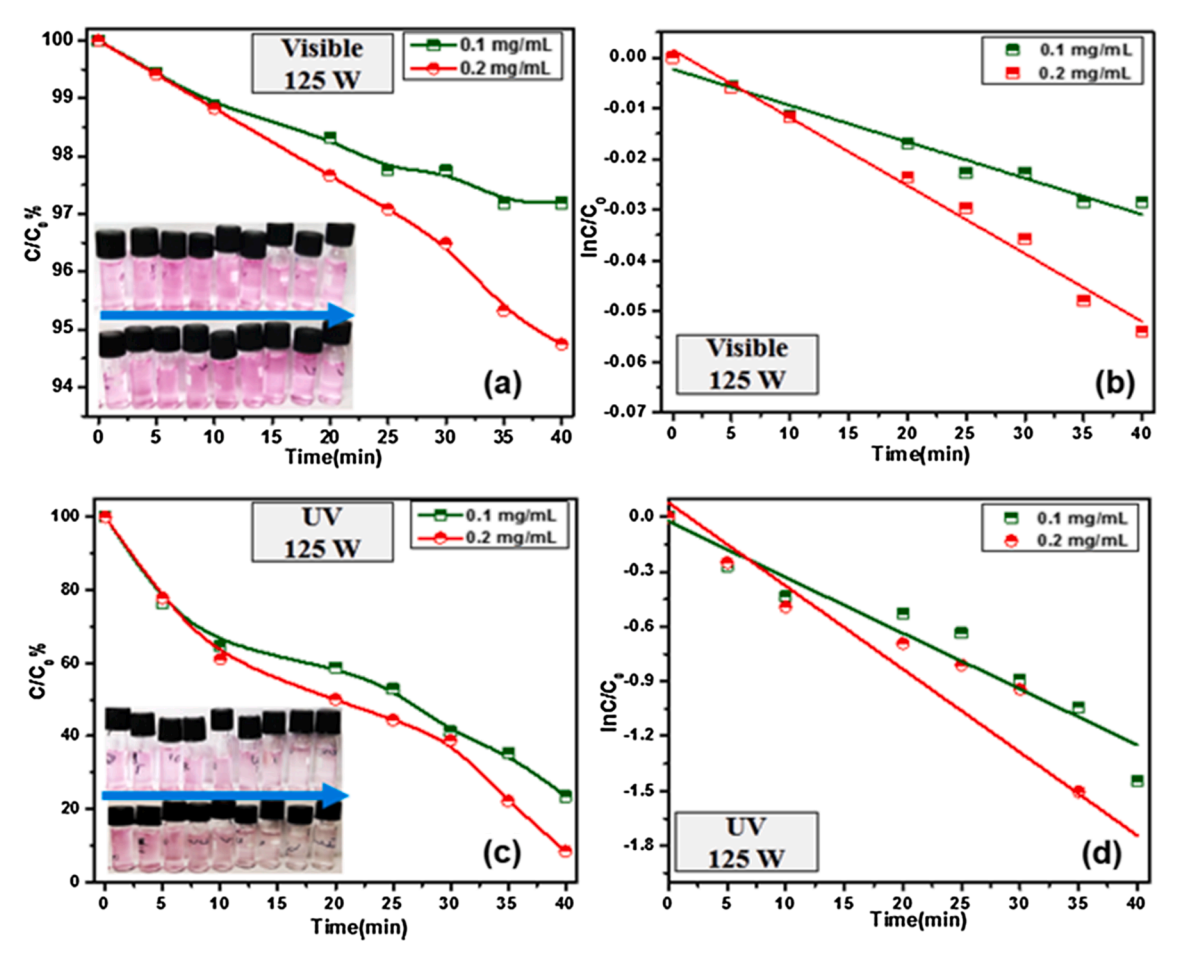


Fig. 8. Photocatalytic degradation of RhB by GZnTPs: (a) change in dye concentration overtime under 125 W visible light; (b) rate kinetics of dye degradation under 125 W visible light; (c) change in dye concentration overtime under 125 W UV light; and (d) rate kinetics of dye degradation under 125 W UV light.

0 2) at $2\theta \approx 26.51^{\circ}$. No impurity peaks are detected in the XRD patterns. Raman spectrum (room temperature, 20 ± 2 °C) of EG exhibits three sharp intense peaks at 1333 cm⁻¹ for D, 1581 cm⁻¹ for G and 2680 cm⁻¹ for 2D (Fig. 5c). The G band peak at 1581 cm⁻¹ is due to the doubly degenerate Zone center (E2g mode of graphite) and related to the inplane vibration of carbon atoms (sp²-bonded). The 2D peak at 2680 cm⁻¹ is due to the second-order zone boundary phonons. The less intense D band peak at 1333 cm⁻¹ is associated with disordered graphite and arises due to the unsatisfied Raman fundamental selection rule of zone-boundary phonons [47]. For hexagonal wurtzite, ZnO shows the optical phonons at the Γ point of the Brillouin zone and are ascribed A1 + 2B1 + E1 + 2E2 [48]. A1 and E1 polar modes are both infrared and Raman active, whereas the B1 modes are both infrared and Raman inactive. Moreover, A1 and E1 modes can be split into transverse (TO) and longitudinal optical (LO) phonons. A sharp and dominant E2 (high) mode located at $445 \, \mathrm{cm}^{-1}$ is the intrinsic Raman active mode of wurtzite hexagonal ZnO, which is a nonpolar mode associated with oxygen displacement. The weak peak at 341 cm⁻¹ may correspond to the multiphonon scattering process of (E₂ (high)-E₂ (low)) and one at 390 cm⁻¹ to A1 (TO). The Raman mode observed at 555 cm⁻¹ can be assigned to A1 (LO) mode. Thus, the presence of high intense E2 (high) mode and suppressed E1 (LO) mode indicate that the synthesized ZnTPs possess crystalline nature with a hexagonal wurtzite structure. The Raman spectra of GZnTPs clearly show the graphene and ZnTPs fingerprints. In addition, I_D/I_G ratio has increased from 0.90 to 0.19, indicating the reduction of oxygen species from EG attached during the exfoliation of NFG. The number of layers can be calculated by the Lorentz fitting of the 2D peak of Raman spectrum [49]. Here, 2D peak (2682 cm⁻¹) is wellfitted by six Lorentz curves (2625, 2639, 2661, 2678, 2689, and 2711

cm⁻¹) with R² accuracy of 0.97533 (Fig. 5d) which indicates that the trilayer graphene system has been successfully formed. This supports the TEM analysis of the tri-layer graphene system (Fig. 4d). The functional groups present in EG, ZnTPs, and GZnTPs were analyzed with FTIR spectroscopy (Fig. 6a). In the FTIR spectrum of EG (Fig. 6a-i), the peak at 3410 cm⁻¹ corresponds to the O-H group (phenolic or alcoholic group), the peaks at 2919 and 2850 cm⁻¹ correspond to C-H vibration, the peak at 1731 cm⁻¹ corresponds to C=O vibration, one at 1633 cm⁻¹ corresponds to C=C vibration, those at 1451 and 1373 cm⁻¹ correspond to C—O/C—N vibration and ones at 872, and 691 cm⁻¹ correspond to C-O vibration [50]. The FTIR spectrum of ZnTPs (Fig. 6a-ii) exhibits peaks at 534 and 499 cm⁻¹ corresponding to Zn—O bond stretching vibration. The peak at 3461 cm⁻¹ corresponds to —OH group attached to ZnO. Moreover, the FTIR spectra of GZnTPs (Fig. 6a-iii) exhibits peaks at 3376 cm⁻¹ that corresponds to -OH group, the peak at 1574 cm⁻¹ corresponds to C=C vibration, and those at 534 and 499 cm⁻¹ to Zn-O bond stretching vibration. In contrast, oxygen-related peaks at 1451, 1373, 872, and 691 cm⁻¹ (Fig. 6a-i) got suppressed or weakened, indicating the removal of oxygen functionalities from the honeycomb lattice.

UV–Vis spectroscopy was done to analyze the characteristic absorption of EG, ZnTPs, and GZnTPs (Fig. 6b). The spectrum for EG shows a shoulder at 316 nm to indicate n– π * transition of the aromatic C—C ring. While UV–Vis spectrum of ZnTPs shows less intense shoulder at 370 nm. The spectrum of GZnTPs shows a less intense peak at 264 nm that corresponds to GNs. This is due to the change in the electronic configuration of EG during the reduction process. The bandgaps (Eg) of EG, ZnTPs, and GZnTPs have been calculated (Fig. 6b: Inset) by Tauc plot [51]. The Eg of \sim 4.97 eV is observed for EG due to the high amount

Table 1 . The comparison of degradation of dyes by different nanocomposites.

Material	Dye	DC* (mg/L)	PC* (mg)	Irradiation	Power (Watt)	Time (min)	DE* (%)	Source
GNs-ZnO	RhB	_	50	UV	300	60	100	Li et al.[55]
GNs-ZnO	RhB	10	10	UV	100	30	50	Yang et al. [56]
rGO-ZnO	RhB	15	10	UV	350	20	50	Kumar et al. [57]
rGO-ZnO	RhB	-	20	Visible	70	120	97.5	Ramanathan et al. [58]
rGO-ZnO	RhB	10	05	Visible	100	180	86	Moqbel et al. [59]
rGO-ZnO	MO	25	25	UV	15	60	98	Metia et al. [60]
GNs-ZnO	MO	13	25	Sun light	-	210	100	Wang et al. [61]
rGO-ZnO	MB	10	200	UV	300	20	98	Qin et al. [62]
GNs-ZnO	MB	-	50	Visible	300	100	100	Gayathri et al. [63]
rGO-ZnO	MB	05	1500	UV	500	250	88	Lv et al. [64]
GNs-ZnO	RhB	01	20	UV	125	40	91.6	Present work
GNs-ZnO	MO	01	20	UV	125	40	45.43	Present work
GNs-ZnO	MB	01	20	UV	125	40	70.87	Present work

 $^{^{\}circ}$ DC = Dye concentration, PC = Photocatalyst concentration, DE = Degradation efficiency.

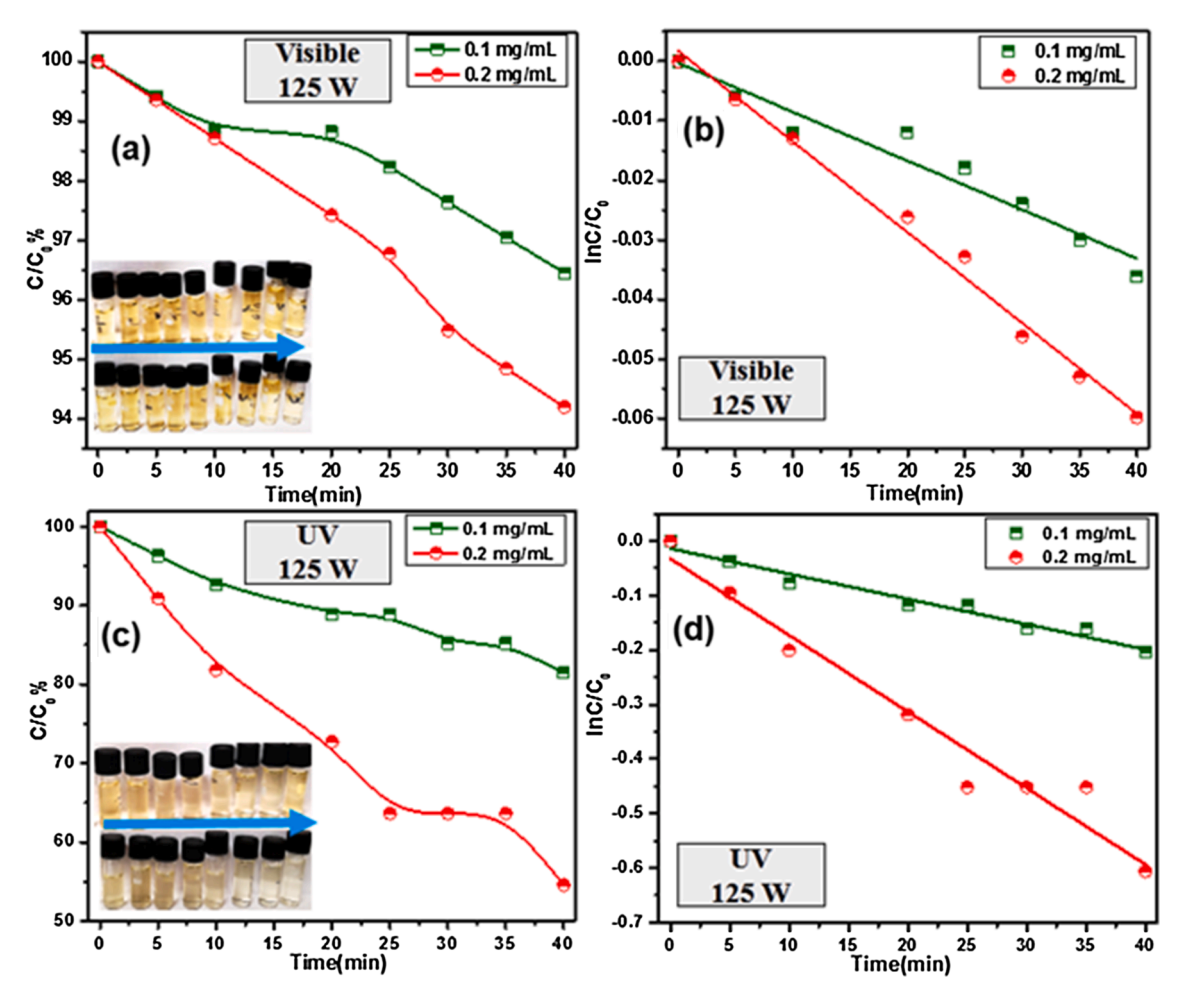


Fig. 9. Photocatalytic degradation of MO by GZnTPs: (a) change in dye concentration with time under 125 W visible light; (b) rate kinetics of dye degradation under 125 W visible light; (c) change in dye concentration with time under 125 W UV light; and (d) rate kinetics of dye degradation under 125 W UV light.

of oxygen functional groups attached during exfoliation of NFG by microwave irradiation. The Eg of $\sim\!3.25$ eV is observed for ZnTPs, and that is close to the reported literature value (3.0–3.3 eV) for Eg of ZnO [21]. The observed Eg of GZnTPs is $\sim\!3.09$ eV.

3.3. Elemental analysis

X-ray photoelectron spectroscopy (XPS) was used to study the surface and composition of EG and GZnTPs (Fig. 7). XPS survey scan (Fig. 7a) shows only C, O, and Zn elements confirming the successful formation of GZnTPs. The deconvoluted—high-resolution XPS C1s

spectrum with Shirley background of EG (Fig. 7b) shows a sharp intense peak corresponding to C—C (284.5 eV) bonds of carbon atoms in 2D planner honeycomb lattice (fitting parameters in SI, Table S2). In addition, other deconvoluted carbon bonding configurations are found at C—O (286.6 eV), C—O (287.1 eV), and C—C—O (288.8 eV).

The presence of different oxygen functional groups (e.g., carboxyl, epoxy, hydroxyl groups) in the EG is marked as reported in the literature [31]. This indicates that a high degree of oxidation has occurred during the exfoliation of graphite. Moreover, a high-resolution spectrum of C1s of GZnTPs (Fig. 7c) suggests that N_2H_4 promotes the reduction of oxygen functional groups present in EG (attached during exfoliation of NFG)

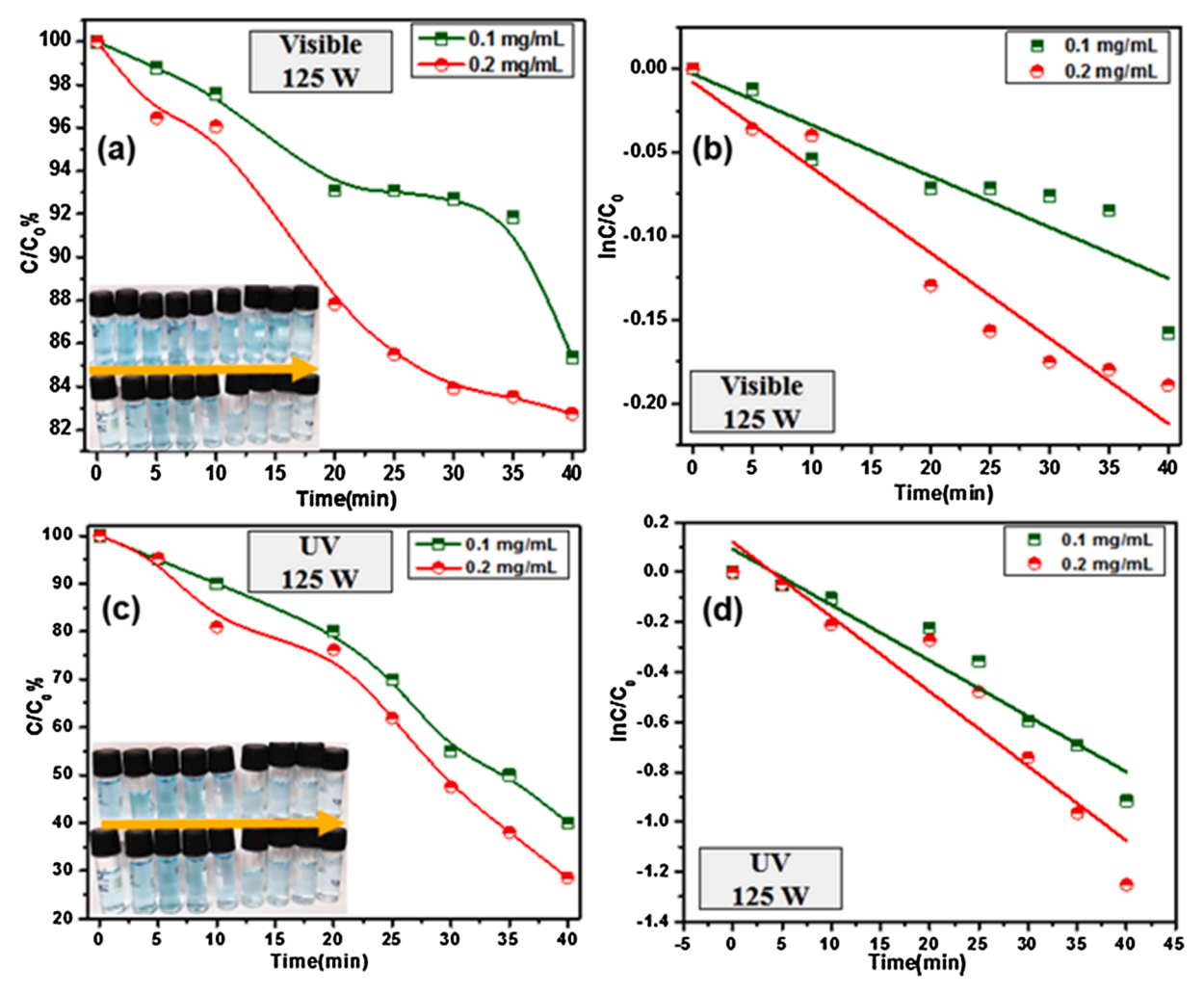


Fig. 10. Photocatalytic degradation of MB by GZnTPs: (a) change in dye concentration with time under 125 W visible light; (b) rate kinetics of dye degradation under 125 W visible light; (c) change in dye concentration with time under 125 W UV light; and (d) rate kinetics of dye degradation under 125 W UV light.

and the oxygen-related peaks are suppressed. In the high-resolution spectrum of Zn 2p, a peak at 1021.70 eV corresponds to Zn $2p_{3/2}$ and another peak at 1044.71 eV corresponding to Zn $2p_{1/2}$ were observed. These peaks were originated from Zn-O bonds (Fig. 7d) [52].

3.4. Photocatalytic activity

The photocatalytic activity of a material depends on various parameters such as type of the semiconductor, light source and intensity, and temperature. The photocatalytic performance of bare semiconducting materials (in our case, ZnTPs) has been found to improve if it is combined with GNs [53,54]. Here, we have analyzed the photocatalytic performance of synthesized GZnTPs (two different concentrations, 0.1 and 0.2 mg/ mL) to degrade organic dyes (RhB, MO, and MB) under 125 W UV and visible light irradiation (SI, Fig. S3, Fig. S4, and Fig. S5). GZnTPs only minimally removed RhB dye under visible light after 40 min (Fig. 8a); the removal was 2.82% with 0.1 mg NCs/mL and that improved only marginally to 5.27% when 0.2 mg NCs/mL was used. In contrast, 76.42% removal was achieved under UV radiation with 0.1 mg NCs/mL and that increased to 91.6% with 0.2 mg NCs/mL (Fig. 8b). Our NCs worked very effectively within a very short time (40 min) compared to work reported by others (Table 1). The NCs could not effectively remove MO under visible light (<6% removal, Fig. 9a). However, once exposed to UV light (Fig. 9b), 0.1 mg NCs/mL degraded 18.48% of MO, and the percentage of degradation increased to 45.48% with 0.2 mg NCs/mL. For MB, the removal under visible light was 14.66% with 0.1 mg NCs/mL, and 17.26% with 0.2 mg NCs/mL (Fig. 10a), and the removal efficiency increased to 59.69% (0.1 mg NCs/mL) and 70.87% (0.2 mg NCs/mL) under UV light (Fig. 10b). Even though MO and MB removal good under UV radiation was not very high, results clearly demonstrate the photocatalytic behavior of the synthesized NCs.

The reaction kinetics of dye (RhB, MO, and MB) degradation have been studied to further understand the photocatalytic activity of the synthesized GZnTPs (Fig. 11). The reactions were found to follow pseudo-first-order kinetics ($-\ln(C_t/C_0) = kt$) where the slope of the liner fitted line gives the rate constant k (min⁻¹), C₀ and C_t correspond to the concentration of dye at the start (initial concentration, t = 0) and at time t, respectively (Fig. 8bd, Fig. 9bd, and Fig. 10bd). It is evident from the results that the maximum value of $k = 0.045 \text{ min}^{-1}$ is found for RhB with 0.2 mg/mL photocatalyst (GZnTPs) concentration under UV irradiation (Fig. 11d) with an associated degradation of 91.6% (Fig. 11b). The highest value of $k = 0.005 \text{ min}^{-1}$ is associated with MB degradation at 0.2 mg/mL photocatalyst concentration under visible light irradiation (Fig. 11c). We compared the relative photocatalytic activity of NCs with that of bare ZnTPs (Fig. S6). The DE has been found to be 59.3, 37.5, and 45.5% for RhB, MO, and MB dyes, respectively with 0.2 mg/mL of bare ZnTPs. The result indicates that GZnTPs NCs are more effective for photocatalytic activity as compared to bare ZnTPs. The comparison of our results with reported literature indicates that our GZnTPs perform better than most NCs in terms of energy input and degradation time (Table 1).

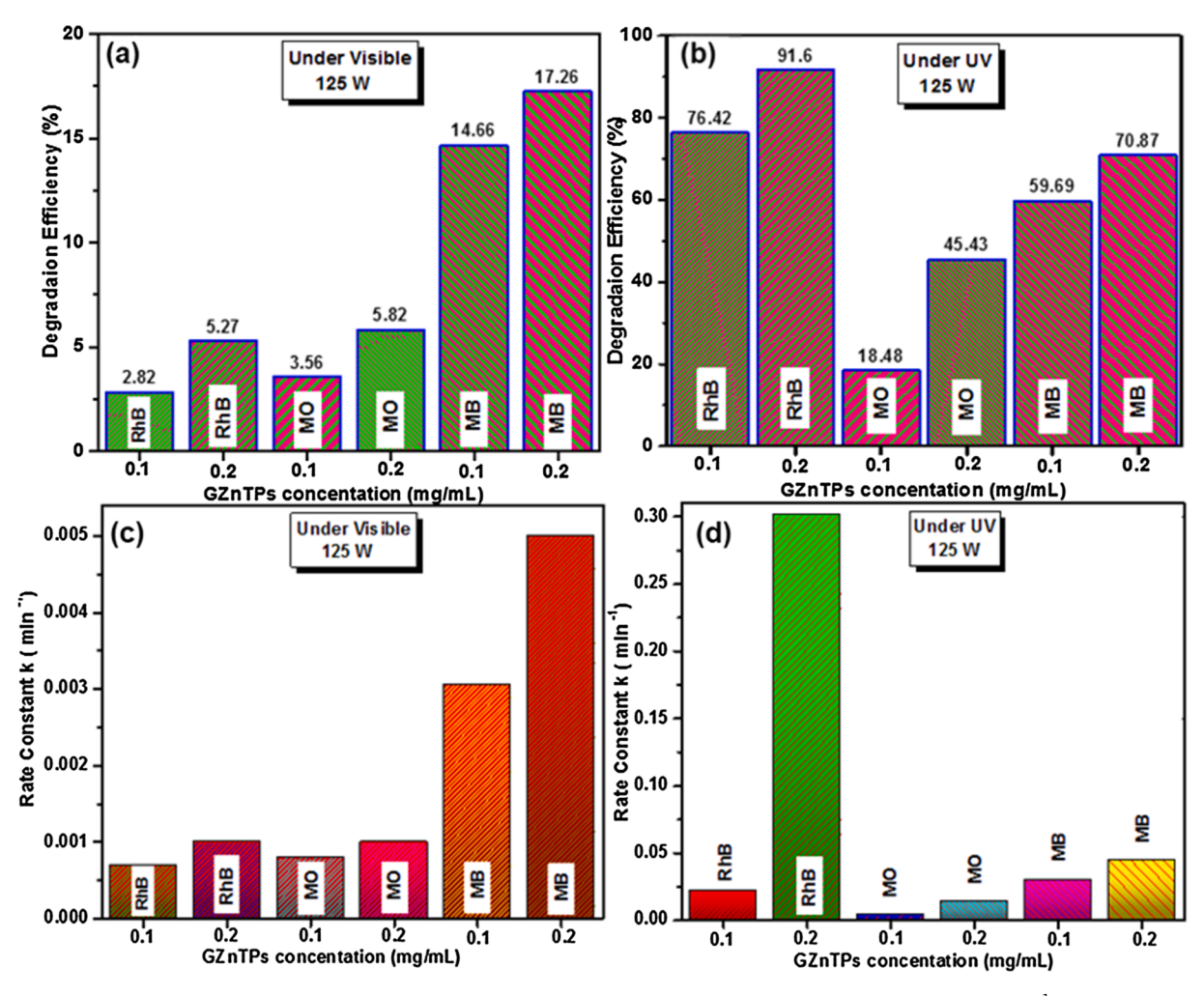


Fig. 11. (a) Degradation efficiency under 125 W visible light; (b) degradation efficiency under 125 W UV light; (c) rate constant k (min⁻¹) under 125 W visible light; and (d) rate constant k (min⁻¹) under 125 W UV light against. The degradation of the three dyes (RhB, MO, and MB) by GZnTPs are represented in the plots.

3.5. Recyclability of GZnTPs

The recyclability of GZnTPs has been studied for RhB, MO, and MB by comparing their photocatalytic activity for several cycles (Fig. 12). In this batch study, 0.2 mg/mL of GZnTPs is added to the dye solution (1 mg/L, 100 mL), and exposed to UV radiation (125 W). The dye concentration in the bulk solution is measured at the end of the experiment and the DE of the GZnTPs is calculated. The filtered GZnTPs are washed and dried at 70 °C and weighed before reusing it for another cycle. The DEs from three such cycles have been compared (Fig. 12d). The recycling studies show that GZnTPs remained effective up to 3 cycles for dyes (Fig. 12abc). It has been found that DE is decreased for RhB from 91.5% (Cycle 1) to 81.7% (Cycle 3). While, the DE is decreased from 45.5% (Cycle 1) to 36.4% (Cycle 3) for MO, it decreased from 70.8% (Cycle 1) to 49.5% (Cycle 3) for MB. The decrease in DEs should be viewed in the context that ~2% of GZnTPs have been lost during the separation process (filtration, washing, drying, and weighing) after each cycle. The results indicate that GZnTPs are reusable for contaminant removal.

3.6. Photocatalytic degradation mechanism

The photocatalytic mechanism for GN-based NC systems is well understood and reported in the literature (Fig. 13) [24], ZnO displays the conduction band at -4.05 eV and valence band at -7.25 eV [65], The work function can be tuned in the range of -4.5 eV to -5.5 eV for GNs produced by reduction techniques [66], This gap in energy level

between ZnO and GNs can create favorable conditions for the direct transfer of electrons from the conduction band of ZnO to GNs. During the UV/Visible light irradiation, the photo-induced electron-hole pairs are generated, and they play a vital role in photocatalytic activity. These photo-generated electrons are transferred to GNs due to their lower energy levels and react with oxygen molecules leading to the formation of reactive oxygen species ($^{\circ}O^{2-}$) [67,68]. This reactive $^{\circ}O^{2-}$ can degrade organic dyes (RhB, MO, and MB) easily. The photo-generated holes also can react with OH– ions to produces hydroxyl radicals ($^{\circ}OH$). The generated $^{\circ}OH$ acts as a strong oxidizing agent to degrade dyes (Eqs. (4)–(9)). GN-based NC systems not only offer a larger surface area but also hinder the charge recombination [25], and that leads to excellent photocatalytic activity.

$$ZnO + h\upsilon \rightarrow ZnO (h^+ + e^-)$$
 (4)

$$ZnO(e^{-}) + GNs \rightarrow ZnO + GNs(e^{-})$$
 (5)

GNs (e⁻) + O₂
$$\rightarrow$$
 O²⁻ + GNs (6)

$$^{\bullet}O^{2-} + H^{+} \rightarrow ^{\bullet}OH \tag{7}$$

$$h^{+} + H_{2}O \rightarrow OH + H^{+}$$
 (8)

$$h^+ + OH + O^{2-} + Organic dyes \rightarrow CO_2 + H_2O$$
 (9)

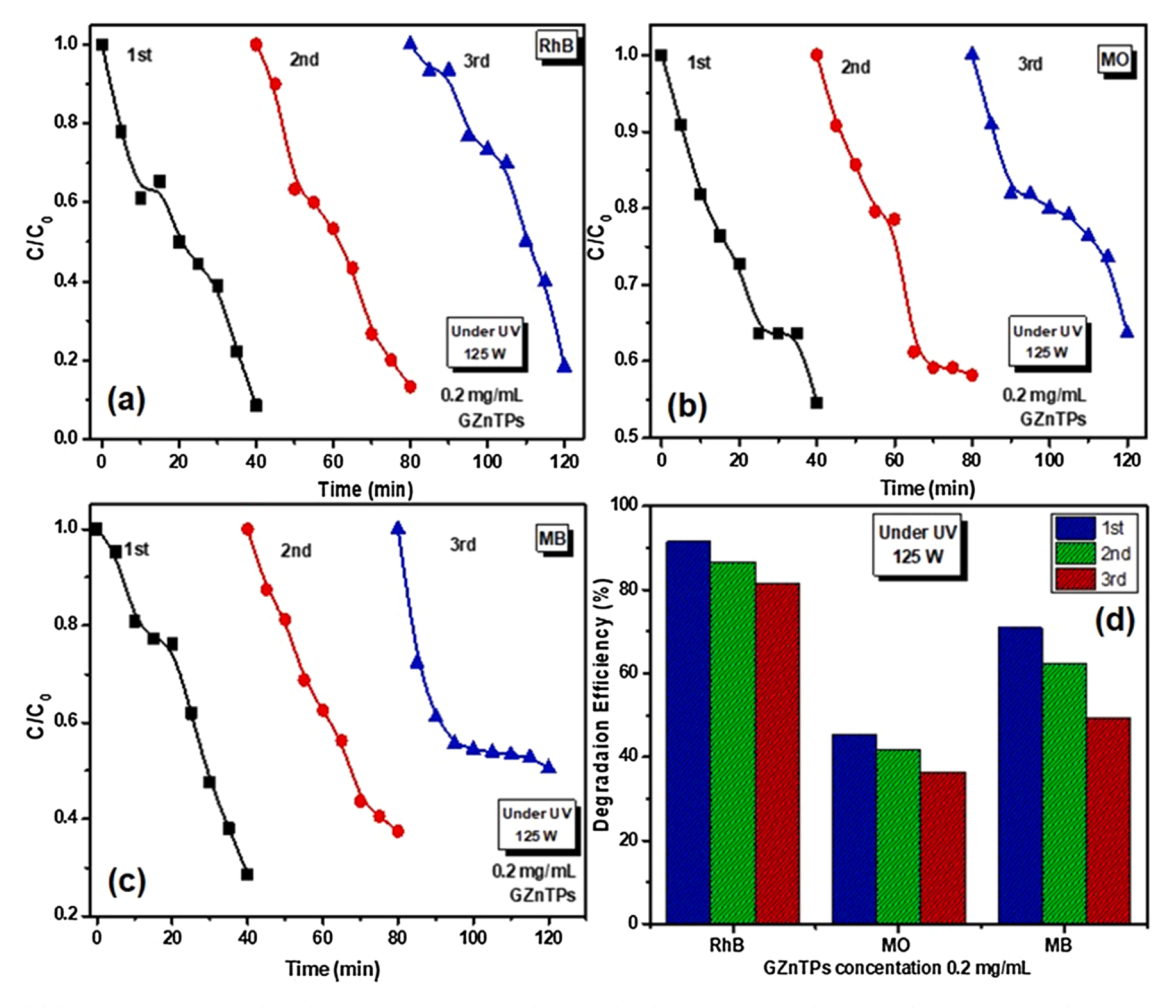
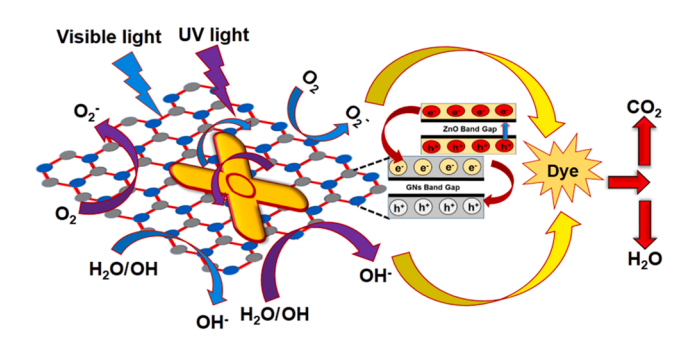


Fig. 12. Recyclability of GZnTPs for the degradation of various organic dyes (a) RhB (b) MO (c) MB, and (c) Degradation efficiency plot up to 3 cycles. All experiments were done under 125 W UV light.



 ${\bf Fig.~13.~} \ \, {\bf The~schematic~illustration~of~the~photocatalytic~mechanism~of~GZnTPs~for~dye~degradation.}$

4. Conclusions

A rapid microwave (300 W, 180 s) solution-phase process has been demonstrated for the successful preparation of graphene-zinc oxide tetrapods nanocomposites (GZnTPs). In this process, N_2H_4 acts as an excellent reducing agent; reduces exfoliated graphene (EG) and zinc precursors simultaneously in a very short period. The reduction of EG and formation of GZnTPs is confirmed by Raman, FTIR, and XPS signatures. The formation of such tetrapods (TPs) is a case of anisotropic faceted growth via the coalescence of ZnO nuclei on the core along the caxis. Further, the growth mechanism for TP structures has been

explained based on the Octa-twin model for crystal growth. The results from organic dye degradation studies indicate that prepared GZnTPs show excellent photocatalytic performance under UV light. Under UV radiation, GZnTPs could degrade various organic dyes (1 mg/L) like Rhodamine B (RhB, 91.6% removal), methylene blue (MB, 71%), and methyl orange (MO, 45%) within 40 min. The GZnTPs show a lower bandgap (3.09 eV) than the bare ZnO TPs (3.25 eV) which may be responsible for effective dye degradation. The synthesized GZnTPs may be explored as a promising photocatalyst due to their reasonable stability (up to 3 cycles) and high photo-degradation efficiency for organic dyes present in water and wastewater. The reported synthesis method can be further explored as a simple one-step technique to grow multifacets nanostructures and composites with controlled dimensions.

CRediT authorship contribution statement

Pankaj Chamoli: Conceptualization, Methodology, Data curation, Formal analysis, Funding acquisition, Writing - original draft, Writing - review & Date : Ravi K. Shukla: Formal analysis, Supervision, Validation, Visualization and Editing. Achintya N. Bezbaruah: Visualization, Supervision, Writing - review & editing. Kamal K. Kar: Conceptualization, Supervision, Writing - review & editing. K.K. Raina: Visualization, Supervision.

Declaration of Competing Interest

The authors declare that they have no known competing financial

interests or personal relationships that could have appeared to influence the work reported in this paper.

Acknowledgment

The authors are thankful to DIT University for the financial support through Seed Money Project No: DITU/R&D/2018/01/Physics. Bezbaruah's visit to DIT University for a part of this research was supported by a Fulbright Specialist Award (2018) and his time on this study at North Dakota State University was supported by a grant from the National Science Foundation (Grant# CBET-1707093).

Appendix A. Supplementary material

Supplementary data to this article can be found online at https://doi.org/10.1016/j.apsusc.2021.149663.

References

- [1] H.H. Naing, K. Wang, P.P. Tun, G. Zhang, Appl. Surf. Sci. 491 (2019) 216–224.
- [2] M.d. Amir, U. Kurtan, A. Baykal, H. Sözeri, J. Mater. Sci. Technol. 32 (2016) 134–141.
- [3] R. Atchudana, T.N.J.I. Edison, S. Perumal, D. Karthikeyan, Y.R. Lee, J. Photochem. Photobiol. B 162 (2016) 500–510.
- [4] J.Y. Zhanga, J.Y. Meia, S.S. Yi, X.X. Guana, Appl. Surf. Sci. 492 (2019) 808.
- [5] R. Atchudana, T.N.J.I. Edison, S. Perumal, D. Karthikeyan, Y.R. Lee, J. Photochem. Photobiol. A 337 (2017) 100–111.
- [6] R. Atchudana, T.N.J.I. Edison, S. Perumal, N. Karthik, D. Karthikeyan, M. Shanmugam, Y.R. Lee, J. Photochem. Photobiol. A 350 (2018) 75–85.
- [7] K.S. Novoselov, V.I. Fal'ko, L. Colombo, P.R. Gellert, M.G. Schwab, K. Kim, Nature 490 (2012) 192–200.
- [8] Appl. Catal. B: Environ. 255 (2019) 117760.
- [9] J. Mater, Chem. A 7 (2019) 17974-17980.
- [10] P. Chamoli, M.K. Das, K.K. Kar, J. Phys. Chem. Solids 113 (2018) 17–25.
- [11] N. Muthuchamy, R. Atchudana, T.N.J.I. Edison, S. Perumal, Y.R. Lee, J. Electroanal. Chem. 816 (2018) 195–204.
- [12] R. Munoz, C. Gomez-Aleixandre, Chem. Vap. Deposition 19 (2013) 297–322.
- [13] K.S. Subrahmanyam, L.S. Panchakarla, A. Govindaraj, C.N.R. Rao, J. Phys. Chem. C 113 (2009) 4257–4259.
- [14] X. Gao, J. Jang, S. Nagase, J. Phys. Chem. C 114 (2010) 832–842.
- [15] Y.L. Zhong, Z. Tian, G.P. Simon, D. Li, Mater. Today 18 (2015) 73-78.
- [16] P. Chamoli, M.K. Das, K.K. Kar, Journal of Applied Physics 122 (2017), 185105.
- [17] V. Dhand, K.Y. Rhee, H.J. Kim, D.H. Jung, J. Nanomater. 14 (2013), 763953.
- [18] P. Chamoli, M.K. Das, K.K. Kar, Physica E 90 (2017) 76–84.
- [19] D.G. Papageorgiou, I.A. Kinloch, R.J. Young, Prog. Mater. Sci. 90 (2017) 75–127.
- [20] C. Hu, T. Lu, F. Chen, R. Zhang, J. Chinese Adv. Mater. Soc. 1 (2013) 21–39.
- [21] J. Wang, R. Chen, L. Xiang, S. Komarneni, Ceram. Int. 44 (2018) 7357–7377.
 [22] A. Kolodziaiczak Padzimska, T. Jacianowski, Materials 14 (2014) 2833–2881.
- [22] A. Kołodziejczak-Radzimska, T. Jesionowski, Materials 14 (2014) 2833–2881.
- [23] K. Qi, B. Cheng, J. Yu, W. Ho, J. Alloys Compd. 727 (2017) 792–820.
- [24] M.A. Johar, R.A. Afzal, A.A. Alazba, U. Manzoor, Adv. Mater. Sci. Eng. 22 (2015), 934587.
- [25] F. Fan, X. Wang, Y. Ma, K. Fu, Y. Yang, Fuller. Nanotub. Car. N. 23 (2015) 917–921.
- [26] K. Ravi, B.S. Mohan, G.S. Sree, I.M. Raju, K. Basavaiah, B.V. Rao, Int. J. Chem. Stud. 6 (2018) 20–26.
- [27] M. Jabeen, M. Ishaq, W. Songz, L. Xu, I. Maqsood, Q. Deng, J. Solid State Sci. Technol. 6 (2017) 36–43.

- [28] N. Kumaresan, M.M.A. Sinthiya, K. Ramamurthi, R.R. Babu, K. Sethuraman, Arab. J. Chem. 13 (2020) 3910–3928.
- [29] J.H. Songcan Wang, B. Yun, T. Luo, P. Butburee, S. Peerakiatkhajohn, M. Thaweesak, L.W. Xiao, J. Mater. Sci. Technol. 33 (2017) 1–22.
- [30] M. Alle, S.H. Lee, J.C. Kim, J. Mater. Sci. Technol. 41 (2020) 168-177.
- [31] P. Chamoli, M.K. Das, K.K. Kar, Graphene 2 (2015) 56-60.
- [32] D. Bhat, Nanoscale Res. Lett. 3 (2008) 31-35.
- [33] J. Huang, C. Xia, L. Cao, X. Zeng, Mater. Sci. Eng. B 150 (2008) 187-193.
- [34] R. Majithia, J. Speich, K.E. Meissne, Materials 6 (2013) 2497–2507.
- [35] Y.C. Chen, S.L. Lo, Chem. Eng. J. 170 (2011) 411-418.
- [36] Y. Caglar, K. Gorgun, S. Aksoy, Spectrochim. Acta A. 138 (2015) 617-622.
- [37] P. Rai, S.G. Kim, Y.T. Yu, J. Mater. Sci.: Mater. Electron. 23 (2012) 344-348.
- [38] M. Shiojiri, C. Kaito, J. Cryst. Growth 52 (1981) 173-177.
- [39] K. Nishio, T. Isshiki, M. Kitano, M. Shiojiri, Phil. Mag. A. 76 (1997) 889-904.
- [40] M. Fujii, H. Iwanaga, M.S. Ichihara-Takeuch, J. Cryst. Growth 128 (1993) 1095–1098.
- [41] S. Maiti, U.N. Maiti, B.C. Behera, S. Pala, K.K. Chattopadhyay, J. Mater. Chem. C 1 (2013) 4940–4947.
- [42] Y. Zhao, W. Li, L. Pan, D. Zhai, Y. Wang, L. Li, W. Cheng, W. Yin, X. Wang, J.B. Xu, Y. Shi, Sci. Rep. 6 (2016) 32327.
- [43] T. Santhaveesuk, K. Shimanoe, K. Suematsu, S. Choopun, Phys. Status Solidi A 215 (2018) 1700784.
- [44] X. Xiao, B. Han, G. Chen, L. Wang, Y. Wang, Sci. Rep. 7 (2017) 40167.
- [45] N. Sykam, R.K. Gautam, K.K. Kar, Polym. Eng. Sci. 55 (2015) 917-923.
- [46] M.F. Khan, A.H. Ansari, M. Hameedullah, E. Ahmad, F.M. Husain, Q. Zia, U. Baig, M.R. Zaheer, M.M. Alam, A.M. Khan, Z.A. AlOthman, I. Ahmad, G. Md Ashraf, G. Aliev, Sci. Rep. 6 (2016) 27689.
- [47] A.C. Ferrari, D.M. Basko, Nat. Nanotechnol. 8 (2013) 235-246.
- [48] Q. Xu, Q. Cheng, J. Zhong, W. Cai, Z. Zhang, Z. Wu, F. Zhang, Nanotechnology 25 (2014) 055501.
- [49] A.C. Ferrari, J.C. Meyer, V. Scardaci, C. Casiraghi, M. Lazzeri, F. Mauri, S. Piscanec, D. Jiang, K.S. Novoselov, S. Roth, A.K. Geim, Phys. Rev. Lett. 97 (2006) 187401.
- [50] B. Xue, L. Ji, J. Deng, J. Zhang, Polym. Eng. Rev. 38 (2018) 167–177.
- [51] J. Tauc (Ed.), Amorphous and Liquid Semiconductor, Plenum Press, New York, 1974.
- [52] R. Khokhra, B. Bharti, H. Lee, R. Kumar, Sci. Rep. 7 (2017) 15032.
- [53] Z.K. Bolaghi, S.M. Masoudpanah, M. Hasheminiasari, Mater. Res. Bull. 115 (2019) 191–195.
- [54] P. Benjwal, M. Kumar, P. Chamoli, K.K. Kar, RSC Adv. 5 (2015) 73249-73260.
- [55] B. Li, H. Cao, J. Mater. Chem. 21 (2011) 3346-3349.
- [56] Y. Yang, L. Ren, C. Zhang, S. Huang, T. Liu, A.C.S. Appl, Mater. Interfaces 3 (2011) 2779–2785.
- [57] B. Saravanakumar, R. Mohan, S. Kim, Mater. Res. Bull. 48 (2013) 878-883.
- [58] S. Ramanathan, S.P. Selvin, A. Obadiah, A. Durairaj, P. Santhoshkumar, S. Lydia, S. Ramasundaram, S. Vasanthkumar, J. Environ, Health Sci. 17 (2019) 195–207.
- [59] R.A. Moqbel, M.A. Gondal, T.F. Qahtan, M.A. Dastageer, Mater. Res. Express 5 (2018), 035050.
- [60] S. Metia, M.R. Rahman, M.I. Ahmad, K.U. Bhat, Appl. Surf. Sci. 451 (2018) 67–75.
- [61] L. Wang, Z. Li, J. Chen, Y. Huang, H. Zhang, H. Qiu, Environ. Pollut. 249 (2019) 801–811.
- [62] J. Qin, X. Zhang, C. Yang, M. Cao, M. Ma, R. Liu, Appl. Surf. Sci. 392 (2017) 196–203.
- [63] S. Gayathri, P. Jayabal, M. Kottaisamy, V. Ramakrishnan, J. Appl. Phy. 115 (2014), 173504.
- [64] T. Lv, L. Pan, X. Liu, Z. Sun, Catal.Sci. Technol. 2 (2012) 2297–2301.
- [65] V. Srikant, D.R. Clarke, J. Appl. Phy. 83 (1998) 5447.
- [66] Y. Shi, K.K. Kim, A. Reina, M. Hofmann, L. Li, J. Kong, ACS Nano 4 (2010) 2689–2694.
- [67] V.P. Lakshmi, V. Rajagopalan, Sci. Rep. 6 (2016) 38606.
- [68] S.P. Lonkar, V.V. Pillai, S.M. Alhassan, Sci. Rep. 8 (2018) 13401.